The Journal of Experimental Biology 213, 4278-4290

doi:10.1242/jeb.047647

Functional morphology and three-dimensional kinematics of the thoraco-lumbar region of the spine of the two-toed sloth

John A. Nyakatura* and Martin S. Fischer

Institut für Spezielle Zoologie und Evolutionsbiologie mit Phyletischem Museum, Friedrich-Schiller-Universität, D-07743 Jena, Germany

*Author for correspondence (john.nyakatura@uni-jena.de)

Accepted 25 September 2010

SUMMARY

Given the importance of thoraco-lumbar spine movements in the locomotion of mammals, it is surprising that *in vivo* three-dimensional (3-D) data on the intervertebral movement of the mammalian thoraco-lumbar vertebral column during symmetrical gaits is limited to horses and dogs. To test whether kinematic patterns similar to those published for these cursorial species are also present during a contrasting mode of quadrupedalism, we quantified thoraco-lumbar intervertebral movements, the resulting pelvic displacements and relative femoral movements during the trot-like steady-state suspensory quadrupedal locomotion of the two-toed sloth (Xenarthra, *Choloepus didactylus*). Scientific rotoscoping, a new, non-invasive approach that combines synchronous biplanar high speed X-ray videos and the reconstruction of skeletal elements from computed tomography bone scans, was used to quantify 3-D kinematics. An analysis of vertebral anatomy and epaxial muscle topography suggests that the thoraco-lumbar spine of sloths is well suited to producing lateral bending and long-axis rotation, but limits powerful sagittal extension. Sloths exhibit complex 3-D movements in the thoraco-lumbar spine that are comparable to those observed in other arboreal quadrupedal mammals. Monophasic lateral bending and long-axis rotation, biphasic sagittal bending and maximal amplitude of sagittal bending at the lumbo-sacral joint were also found in other quadruped mammals and may represent general aspects of mammalian symmetric gaits. Maximal amplitude of lateral bending and long-axis rotation vary in regard to the vertebral level. It is suggested that a cranio-caudal pattern of angular deflections of the spine results from the out-of-phase movement of diagonal forelimbs and hindlimbs in other walking gaits, because it is not evident in the trot-like locomotion analyzed here. The analysis also illustrates the difficulties that arise when lumbar movement is deduced from intervertebral joint morphology alone.

Key words: intervertebral joint, vertebral column, XROMM, scientific rotoscoping, pelvis, femur, *Choloepus didactylus*, Xenarthra.

INTRODUCTION

Movements of the vertebral column are of fundamental significance in the locomotion of mammals, because they have been shown to contribute significantly to propulsion (e.g. Howell, 1944). The most substantial movement of the vertebral column during symmetrical gaits of mammals is a monophasic lateral bending that results in maximal lateral displacement of the pelvis to either side at touch-down of the hindlimb of the same side of the body (Shapiro et al., 2001). Secondly, there occurs a less pronounced, biphasic sagittal bending. Maximal sagittal flexion occurs at hindlimb touch-down whereas maximal extension occurs at hindlimb lift-off (Schilling and Fischer, 1999; Faber et al., 2000; Ritter et al., 2001; Licka et al., 2001). Thirdly, there is axial rotation about the long-axis of the spine, which is more pronounced in symmetrical gaits than in asymmetrical gaits (Faber et al., 2000). The pelvis is thus displaced three dimensionally (3-D) during symmetrical gaits in mammalian locomotion (cf. Jenkins and Camazine, 1977).

In view of the importance of these 3-D axial movements in mammalian symmetrical gaits, it is surprising that the kinematic data available on the body axis are limited. Although published quantifications of 3-D pelvic displacements during symmetric mammalian quadrupedalism are themselves scant (Jenkins and Camazine, 1977; Schilling and Fischer, 1999; Wennerstrand et al., 2004; Schmidt, 2005), the minute intervertebral movements associated with these displacements are even less well investigated. Efforts have been made to deduce intervertebral mobility from the morphology of the vertebrae (e.g. Slijper, 1946; Boszczyk et al., 2001). However, only a fraction of the possible *in vitro* mobility of the musculo-skeletal system or of the mobility at non-locomotor activities such as grooming, fighting or mating can be expected during cyclic locomotion (Fischer, 1998). Additionally, in at least one available example of experimental *in vivo* motion analysis, the movements observed were greater than expected on the basis of the articular features (Haussler et al., 2001).

Because 3-D intervertebral movements are difficult to observe, necessitating 3-D *in vivo* methods, data relating to these movements have only been published for horses (Haussler et al., 2001) and, to a limited extent, dogs (Wood et al., 1992; Schendel et al., 1995) – both highly cursorial mammals adapted to sustained running. These few studies relied on the invasive instrumentation of the vertebrae analyzed.

In kinematic studies on the back movements of horses during a slow lateral sequence walk, maximal intervertebral lateral bending was observed to occur earlier between the lumbar vertebrae than between the more cranial thoracic intervertebral joints, whereas in a trotting gait this shift was not evident (Faber et al., 2000; Haussler et al., 2001). Accordingly, Schilling and Carrier documented sequential electromyographical (EMG) activation patterns in the back muscles of dogs during walking and galloping, but synchronized activity during trotting (Schilling and Carrier, 2010). The authors concluded that the cranio-caudal EMG patterns of dogs are consistent with a traveling wave of trunk bending in walking

gaits and with a standing wave of trunk bending in trotting gaits (Schilling and Carrier, 2010). Kinematic data and EMG data thus imply a close relationship between footfall pattern and the 3-D movements of the vertebral column during symmetric gaits. Furthermore, published studies on the 3-D axial movement of quadrupedal mammals have shown that there are regional differences in the magnitude and pattern of the three axial rotations: lateral bending about a dorso-ventral axis, sagittal bending about a latero-lateral axis and long-axis rotation about a longitudinal axis (Haussler et al., 2001).

If previously published patterns of 3-D axial movement during symmetric mammalian quadrupedalism are also present in a contrasting type of symmetric locomotor behavior, they are likely to represent a more general pattern. To this end, we present here an *in vivo* analysis of 3-D thoraco-lumbar intervertebral movements during suspensory quadrupedal locomotion in the two-toed sloth (Xenarthra, *Choloepus didactylus*, Linné 1758). The following statements reflect what we would expect with regard to the movements in the thoraco-lumbar spine of the two-toed sloth during suspensory quadrupedal locomotion on the basis of data available on horses and dogs:

1. Lateral bending will be monophasic and maxima will occur to either side associated with touch-down events of the hindlimbs.

2. Sagittal bending will be biphasic and maxima of flexion will be associated with touch-down events of the hindlimbs, whereas minima will occur at instances of hindlimb lift-off.

3. Long-axis rotation will be monophasic and maximal rotations towards one side of the body will be associated with touch-down of the ipsilateral hindlimb, whereas minima will occur at lift-off of the ipsilateral hindlimbs.

4. Amplitudes of intervertebral angular deflections will be highest at the lumbo-sacral joint.

5. Owing to the trot-like footfall pattern that sloths utilize during steady-state locomotion, i.e. diagonal limbs move approximately in synchrony (Nyakatura et al., 2010), no cranio-caudal phase shift is expected in the timing of the maximal amplitudes of intervertebral angular deflection.

In addition, the 3-D movements of the axial skeleton and the resulting displacements of the pelvis will have a displacing effect on the pivot of the femur (cf. Jenkins and Camazine, 1977). 3-D femoral movements relative to the pelvis are seldom quantified (but see Rubenson et al., 2007; Kubo and Ozaki, 2009) because of the difficulty of placing an anatomical coordinate system at the hip joint to obtain this data. Having said this, kinematic data on femoral movement are often used to interpret, among other things, EMG data from limb muscles. In this publication, we quantify thoraco-lumbar movement, pelvic displacement and femoral movement relative to the pelvis.

Our *in vivo* 3-D analysis was performed using 'scientific rotoscoping' (Gatesy et al., 2010), a new, non-invasive, markerless X-ray reconstruction of moving morphology [XROMM (Brainerd et al., 2010)] approach that combines synchronous biplanar high-speed X-ray videography and the 3-D reconstruction of skeletal elements from computed tomography (CT) bone scans (Fig. 1). The kinematic results will be discussed in relation to the skeletal anatomy and characteristics of the epaxial musculature of the thoraco-lumbar vertebral spine.

MATERIALS AND METHODS

All experiments and procedures were registered with the Committee for Animal Protection of the State of Thuringia, Germany, and were conducted in accordance with its guidelines (Reg. no. 02-08/04).

Anatomical investigation

Anatomical investigation was undertaken on a female cadaver of *C. didactylus* donated by Dresden Zoo (Germany). After dissection to study the epaxial muscular topography, the cadaver was macerated and the vertebrae of the thoraco-lumbar spine were photographed to document the intervertebral joint configuration of the two-toed sloth. In this paper we use the anatomical nomenclature of the Federative Committee on Anatomical Terminology (FCAT, 2008).

The subjects used in the anatomical investigation and the motion analysis (see below) have been used in previous studies and have been shown not to have uncharacteristic morphologies. Their morphometric parameters were within 1 s.d. of a larger sample that was composed of museum material (Nyakatura and Fischer, 2010). Neither the female [10.6 kg, 87 cm in length (measured from the anterior tip of nose to the ischium)] nor the male (6.5 kg, 78 cm) displayed any peculiarities.

Experimental setup for biplanar high-speed X-ray video recordings

The experimental setup for obtaining synchronous biplanar X-ray videos was described in detail in a previous publication (Nyakatura et al., 2010). Briefly, we recorded synchronous, digital high-speed X-ray videos from the dorso-ventral and latero-lateral perspectives during steady-state locomotion in two individuals (Fig. 1). Both 40 cm diameter image intensifiers were equipped with a Visario Speedcam^{TM} (Weinberger GmbH, Erlangen, Germany) and recorded at a resolution of 1536×1024 pixels and a frame rate of 300 frames s^{-1}. Any distortion of X-ray images was corrected with the help of a Matlab^{TM} workflow developed by the XROMM group (Brown University, Providence, Rhode Island, USA). Images were undistorted by recording the X-ray image of a standardized perforated metal grid and subsequently using the idealized geometry of the perforations to correct the frames of the X-ray videos (Brainerd et al., 2010).

A calibration object made of acrylic glass (20×12×12 cm) with metal spheres inserted at 1 cm distances was also recorded in the same experimental setup. The spheres needed to be identified on both recorded projections to enable us to calibrate the 3-D space covered by the two X-ray devices, which we did using an 11-parameter direct linear transformation Matlab^{TM} program (DLT; necessary Matlab^{TM} files available at www.xromm.org), also developed by the XROMM group at Brown University (Brainerd et al., 2010).

To facilitate the recording of several consecutive strides, the sloths were trained to move along a motor-driven 'treadpole' (4000×40 mm) in front of the image intensifiers. All trials slower than 0.2 m s^{-1} and faster than 0.3 m s^{-1} were discarded and only strides with symmetry values (i.e. the percentage of a given hindlimb cycle at the instant of contralateral hindlimb touch-down) between 0.4 and 0.6 were analyzed for the sake of uniformity. We used the Student's *t*-test for independent samples (analyses carried out in SPSS^{TM} 12.0, IBM Corporation, Somers, NY, USA) to test whether both individuals differed significantly with regard to gait parameters in different strides (sample size N=14 and 18, respectively; Table 1). Variation of gait parameters within individuals was greater than the variation between individuals; therefore, stride cycles from both individuals were pooled. Ten steady-state stride cycles for each study subject were analyzed. All trials were time normalized to 50 points over the contact phase and swing phase, respectively, to facilitate the compilation of multiple strides so that the mean and standard deviation of the kinematic data could be determined.

Table 1. Inter- *versus* intra-individual variability in gait parameters for *Choloepus didactylus*

Parameter	Male individual	Female individual	Both individuals	Comparison between individuals (*P*-value)
Stride length (cm)	58.8±5.0 (*N*=18)	60.2±5.9 (*N*=14)	59.5±5.3 (*N*=32)	0.480 n.s.
Hindlimb swing phase duration (sec)	0.65±0.2 (*N*=18)	0.7±0.1 (*N*=14)	0.67±0.2 (*N*=32)	0.407 n.s.
Hindlimb contact phase duration (sec)	1.62±0.3 (*N*=18)	1.68±0.2 (*N*=14)	1.66±0.2 (*N*=32)	0.702 n.s.
Femur touch-down angle (deg)	39.0±5.1 (*N*=10)	34.7±5.2 (*N*=10)	36.9±5.4 (*N*=20)	0.077 n.s.

Data are means ± s.d. No statistically significant differences were observed and all trials were subsequently pooled and analyzed together.
n.s., not significant.

X-ray reconstruction of moving morphology (XROMM)

CT scans of disarticulated skeletal elements were performed using a GE Lightspeed 16 CT scanner (GE Healthcare, Munich, Germany) at the Zentralklinik, Bad Berka, Germany, at 120 kV and 150 mA. To reconstruct bone models, raw data were surface-rendered in Imaris™ 6.4 (Bitplane AG, Zurich, Switzerland), converted into the .obj file format using customized software (by H. Stark, available at www.stark-jena.de). Models were imported into Maya™ 8.0 (Autodesk GmbH, Munich, Germany) and hierarchically connected *via* virtual joints to form a digital marionette. To protect the living animals from the risks associated with anesthesia, a different skeleton was scanned and then scaled to match the size of the living subjects using reference X-ray images (cf. Gatesy et al., 2010).

In Maya™, virtual dorso-ventrally and latero-laterally oriented cameras were created and their relative position in virtual 3-D space was calibrated so that they imitated the actual X-ray sources (the necessary Maya™ embedded language files are available at www.xromm.org) (Fig. 1).

If, in the hierarchical joint chain a higher-order skeletal element is moved, all lower ranked skeletal elements are passively displaced. The movements of skeletal elements are reported relative to higher-order skeletal elements in the hierarchical joint chain (Table 2). Displacement of the pelvis (top rank in hierarchy) is reported relative to a global coordinate system, with positive *x* in the direction of movement, positive *y* in the ventral direction and positive *z* to the animal's left. Right-handed anatomical coordinate systems were implemented at the pelvis, at the pivot of the femur and at the six caudal-most presacral joints (in the center of the intervertebral discs). In each case, the *x*-axis is oriented along the long axis of the bone whose movement is being measured and the *z*-axis is oriented to reflect its main axis of rotation. The zero-positions of rotations are not natural, but idealistic positions aligned to the global coordinate system (Table 2). We were forced to restrict the analysis to the six caudal-most presacral vertebrae because of the limited size of the field of vision of the two X-ray cameras. Intervertebral movements are reported by describing the motion of a cranial vertebra relative to the vertebra immediately caudal (cf. Haussler et al., 2001). Although 3-D kinematics always consist of three rotations (about the *x*-, *y*- and *z*-axes) and three translations (along the *x*-, *y*- and *z*-axes), translations between vertebrae, in the lumbo-sacral joint and in the hip joint were found to be very small (less than our analytical accuracy, see below) and are therefore ignored in this study.

During scientific rotoscoping, the digital marionette was positioned to match the X-ray shadow of the two projections in every fifth frame. After a trial was completed, the three rotations representing the movement of a bone relative to the higher-order skeletal element were exported into Microsoft™ Excel.

Scientific rotoscoping is an iterative process and quality largely depends on the skill of the investigator, although the accuracy of the 3-D representation of the experimental scene within Maya™ and the repeatability of measurements also play a role. Accuracy and

Table 2. Anatomical coordinate systems used for kinematic analysis in *Choloepus didactylus*

Joint/element (hierarchy)	Anatomical significance of rotation about axis	Zero-point for rotations
Global coordinate system (top)		
x-axis	–	–
y-axis	–	–
z-axis	–	–
Pelvis (1st order)		
x-axis	Long-axis rotation of pelvis (roll)	Aligned with global *x*
y-axis	Lateral displacement of pelvis (yaw)	Aligned with global *y*
z-axis	Sagittal protraction/retraction of pelvis (pitch)	Aligned with global *z*
Femoral pivot/femur (2nd order)		
x-axis	Long-axis rotation of the femur	Femur is not rotated (lateral and medial condyles aligned to global *y*-axis)
y-axis	Abduction relative to the pelvis	Femur is not abducted
z-axis	Protraction and retraction relative to the pelvis	Femur is parallel to global *x*-axis
Pre-sacral joints/3rd lumbar to 21st thoracic vertebrae (2nd to 7th order)		
x-axis	Rotation about long axis of the spine (negative rotation decreases the distance from reference hip joint to support)	Vertebrae are not rotated
y-axis	Lateral bending (negative towards body side of reference hindlimb)	Vertebrae are orientated along the long axis of spine (global *x*)
z-axis	Sagittal bending (degree of flexion from zero point)	Vertebrae are orientated along global *z*

Right-handed coordinate systems are implemented for each joint with the *x*-axis oriented along the long axis of adjacent bone and the *z*-axis always oriented to represent the most distinct motion of adjacent bone. The *y*-axis is perpendicular to the other two axes. For the global coordinate system, positive *x* is in the direction of movement, positive *y* is towards dorso-ventral image intensifier and positive *z* is to the animal's left.

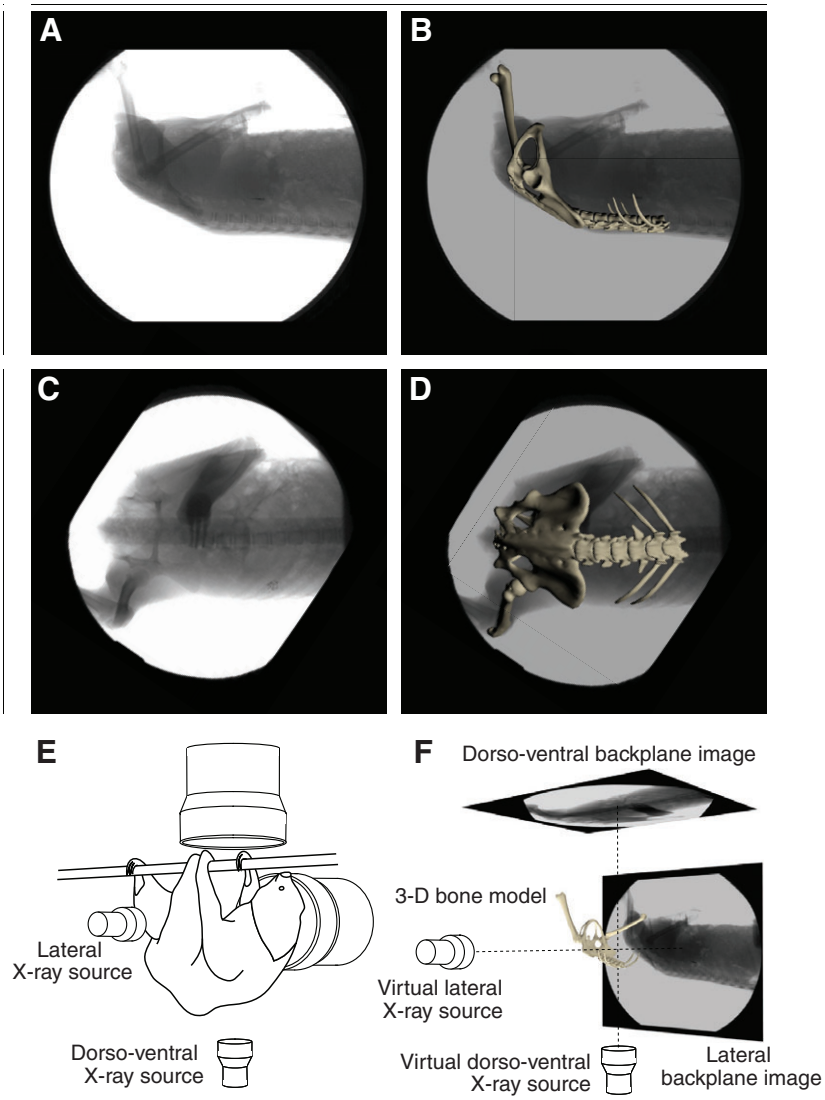

Fig. 1. Scientific rotoscoping (Gatesy et al., 2010). A virtual marionette is positioned to match the X-ray shadow of synchronously recorded latero-lateral (A,B) and dorso-ventral (C,D) X-ray videos. This requires the experimental setup (E) to be 3-D calibrated and virtually recreated within the 3-D software Maya™ (F). For further explanation, see Materials and methods.

repeatability are determined by the quality of undistortion, calibration, the visibility of the skeletal structures on the X-ray images and the frame rate of the X-ray videos used. Because of the unequal shape and thickness of the studied structures, no one value can represent the accuracy of all measurements. General accuracy for optimal conditions was measured by comparing the known opening of a pair of vernier calipers (150 mm) to the measured opening following the approach used in this study. We determined the opening to be 150.705 mm within Maya™ – a deviation of <1 mm. To assess repeatability, the femoral orientation relative to the pelvis and rotations at the lumbo-sacral joint at lift off in a single trial were determined on five consecutive days of data analysis and only small deviations (mean ± s.d.) were found. Femoral orientation (rotations relative to the zero-point of measurement) values were as follows: rot x, –28.3±1.45 deg; rot y, –33.0±0.84 deg; and rot z, –62.2±0.46 deg. Rotations at the lumbo-sacral joint were: lateral bending, –2.3±0.21 deg; sagittal bending, 18.3±0.34 deg; and long-axis rotation, 0.9±0.87 deg. To account for this inaccuracy, we decided to round off values to full degrees. However, it does mean that minute movements of <1 deg were not reliably measured. Because the long-axis rotation at the intervertebral joints was particularly difficult to detect, we only measured the long-axis rotation of the intervertebral joints at touch-down, lift-off, mid-contact and mid-swing of each limb (i.e. eight measurements per stride cycle) to reveal the minute movements between these instances. Maya™ then uses a spline curve estimate to connect the measured instances (cf. Gatesy et al., 2010). We also determined the frame in which lift-off occurred on five days of data analysis: frame 153.3±0.75 (i.e. s.d. is less than 1/300 s).

Quantifying the displacing effect of pelvic movements on the trajectory of the knee

Pelvic displacements contribute to step length in symmetrical gaits. XROMM makes it possible to quantify the contribution of pelvic displacements to the overall 3-D displacement of the limb. We conducted 'virtual experiments' and turned off ('muted') the motion of the pelvis or specific aspects of the motion [i.e. pelvic tilt (roll), pelvic protraction/retraction (pitch) or pelvic lateral displacement (yaw)], in the animated trials. The displacing effect of specific motions of the pelvis was then assessed by comparing the knee trajectory of the virtual experiment with the knee trajectory of normal locomotion.

RESULTS

Skeletal anatomy of the thoraco-lumbar spine and pelvic region

Xenarthra are characterized *inter alia* by additional ('xenarthrous') intervertebral articulations in the postdiaphragmatic spine that occur between the enlarged metapophyses and anapophyses (Flower, 1882)

[see Gaudin and McDonald (Gaudin and McDonald, 2008) for a recent review of xenarthran morphology]. However, in extant sloths the anapophyses are only weakly developed (Gaudin and McDonald, 2008) and in *Choloepus* they are not visible at all (Kraft, 1995). *Choloepus didactylus* usually has 23–24 thoracic and 3 lumbar vertebrae (Flower, 1882). In all Xenarthra, the anterior-most vertebrae of the tail are fused to the sacrum, forming a synsacrum. The synsacrum is connected to the ilium (sacro-iliac joint) and also to the ischium (sacro-ischiadic suture). The pelvis thus has two rigid articulations to the vertebral column, which prohibit any motion of the pelvis relative to the spine. Our dissected specimen and our live subjects were no exception.

In *C. didactylus*, the thoraco-lumbar spine has exceptionally short spinal processes that point caudal (Fig. 2). The anterior zygapophyses of the thoracic vertebrae are oriented to face dorsal, whereas those of the last thoracic vertebra and all lumbar vertebrae embrace the posterior zygapophysis of the previous vertebra and have a more medial (parasagittal) orientation. Vertebra TH22 has horizontal anterior but parasagittal posterior zygapophyses and is thus termed the diaphragmatic vertebra (Slijper, 1946). Parasagittal orientation of the zygapophyses is also present at the lumbo-sacral joint. The posterior zygapophyses and the lamina arcus vertebrae of the thoraco-lumbar spine form a relatively flat surface that protrudes caudal into the space between the medially facing anterior zygapophyses of the subsequent vertebra. The configuration of the lumbar vertebrae can be compared to roofing tiles. X-ray images of maximal sagittal extension in a manipulated cadaver revealed that no hyperextension is possible at the thoraco-lumbar spine.

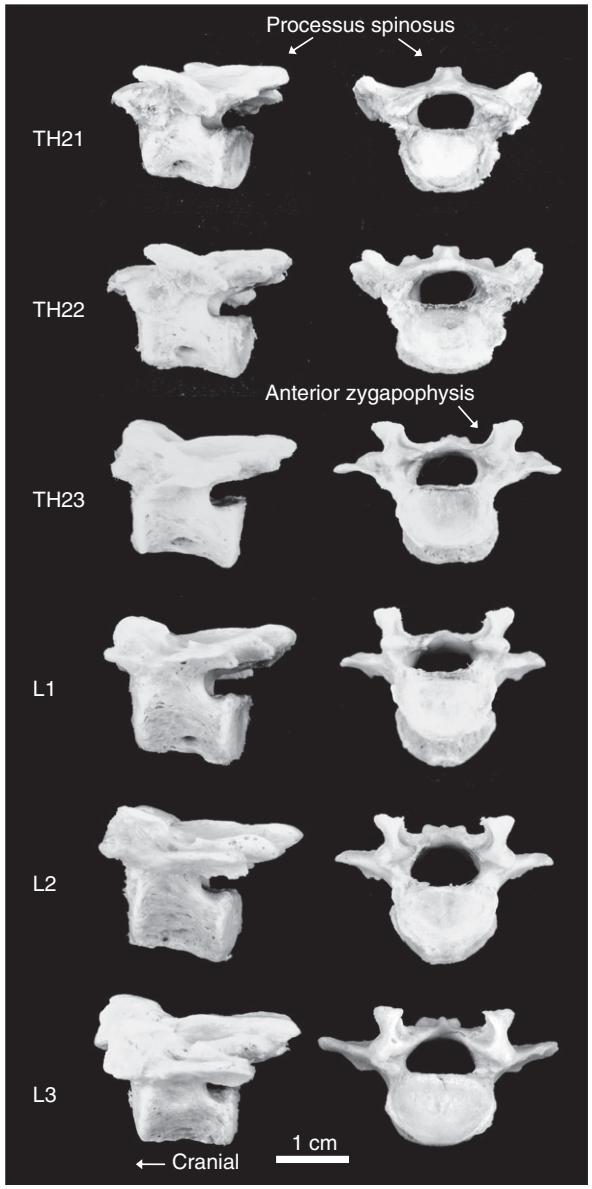

Fig. 2. The six caudal-most presacral vertebrae in *Choloepus didactylus*. Left: cranial aspect; right: lateral aspect. Please note the approximately horizontal articular facets of the anterior zygapophyses of vertebrae TH21 and TH22, and the approximately parasagittal articular facets of the anterior zygapophyses of the last four presacral vertebrae. Also note the very low processus spinosi.

Morphological characteristics of the epaxial musculature at the thoraco-lumbar spine

The m. iliocostalis, m. longissimus dorsi and the transversospinal system are easy to discern in the sloth owing to differences in the orientation of the fascicles or fascia separating these muscles. Overall, the epaxial musculature is remarkably thin. The m. iliocostalis, for instance, only consists of two to three layers of fascicles. A dense fascia thoracolumbalis covers the fascicles of the epaxial muscles.

In the thoraco-lumbar region, the fascicles of the m. iliocostalis lumborum originate from the crista iliaca, from the lamina superficialis of the fascia thoracolumbalis and from an aponeurosis that separates the muscle medially from the m. longissimus dorsi. The fascicles of the lumbar portion of the m. iliocostalis attach to the three caudal-most thoracic vertebrae or to the lamina profunda of the fascia thoracolumbalis that connects the crista iliaca, the processus costales of the lumbar vertebrae and the caudal-most ribs, and extends ventral to the epaxial muscles.

In the lumbar region, the m. longissimus dorsi originates at the fascia thoracolumbalis and extends medially from the fascia that separates this muscle from the transversospinal system. It inserts on the lamina profunda of the fascia thoracolumbalis and on the aponeurosis that separates m. iliocostalis from this muscle. At the thorax, the fascicles attach to the dorsal surface of the ribs proximal to the m. iliocostalis. Fascicle length at the lumbar spine is much more variable than at the thorax, where individual fascicles almost exclusively span two vertebral levels.

We did not attempt to attribute individual fascicles to the separate muscles that make up the transversopinal system because no intramuscular aponeuroses (the structures that separate the different muscles) were observed. In the lumbar region, the fascicles of the transversopinal system originate from the fascia thoracolumbalis, the intramuscular aponeurosis that separates this muscle from the m. longissimus, the medial crista iliaca and the dorsal surface of the sacrum and lumbar vertebrae. The fascicles attach to the remarkably short processus spinosi, the lamina arcus vertebrae of the lumbar and thoracic spine and the processus costales. However, it is important to point out that the general orientation of most fascicles is cranio-medial rather than cranio-lateral. Fascicle lengths are very variable in the transversopinal system, reflecting the variation in the muscles of which they are composed. Lengths vary from fascicles that span only one vertebral level (e.g. mm. rotatores breves) to fascicles that span the complete lumbar spine and directly attach to thoracic vertebrae (m. semispinalis, m. multifidus).

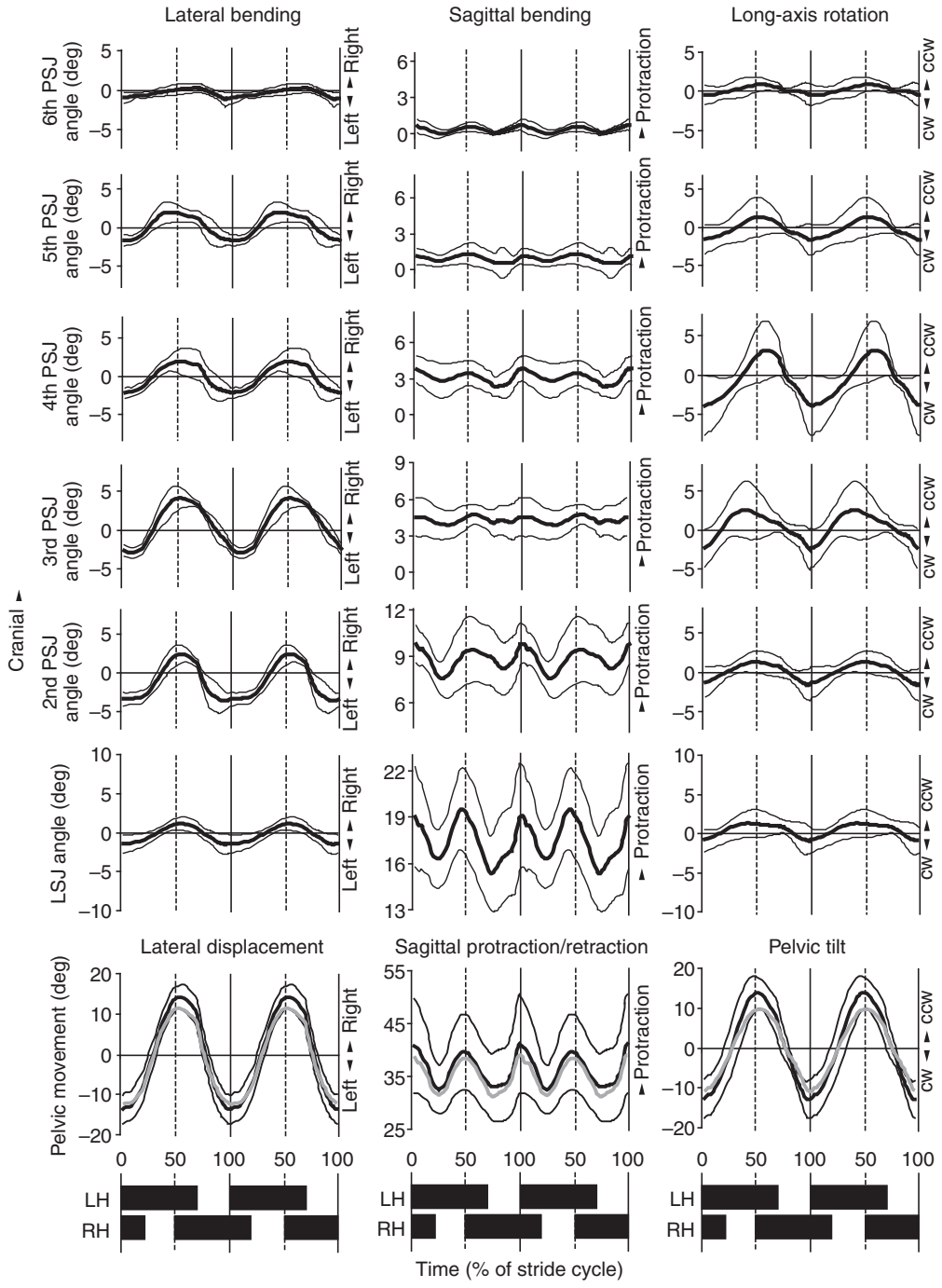

Fig. 3. Mean angular intervertebral movements and pelvic displacements (±s.d.; *N*=20) relative to two consecutive average stride cycles in *Choloepus didactylus*. cw, clockwise as seen from cranial; ccw, counterclockwise as seen from cranial; LSJ, lumbo-sacral joint; PSJ, presacral joint; grey, summation of presacral intervertebral movements. Timing of contact phases (black boxes) and swing phases (white space between boxes) during two mean stride cycles of the left hindlimb (LH) and right hindlimb (RH).

Characteristics of steady-state locomotion in the sloth

Interlimb coordination and the spatio-temporal gait parameters of unrestrained and steady-state locomotion in the two-toed sloth were reported in an earlier publication (Nyakatura et al., 2010). The characteristics of steady-state (treadpole) locomotion are only briefly summarized here. Our analysis of steady-state locomotion was restricted to sequences ranging from 0.2 to 0.3 m s^{-1}. In this speed range, limb kinematics and spatio-temporal gait parameters were relatively uniform and the sloths utilized trot-like diagonal-couplet gaits (diagonal forelimbs and hindlimbs are moved nearly synchronously). The average stride cycle of the hindlimbs during a steady-state trial lasted for a mean ± s.d. of 2.34±0.4 s (*N*=32). Contact ended after 1.66±0.25 s (or 71% of the stride cycle) and stride length was 0.60±0.05 m. On average, touch-down events of hindlimbs were nearly symmetric in analyzed trials, with the contralateral hindlimb touching down at 49±4% of the reference hindlimb's stride cycle. In this study, we proceed on the assumption that touch-down events are symmetric. In sum, during an average hindlimb stride cycle a phase of bilateral support (which lasts until lift-off of the contralateral hind at the 21% mark) is followed by unilateral support (until touch-down of the contralateral hind at the 50% mark), which is followed by bilateral support (until lift-off of the reference hind at the 71% mark) and a final phase of unilateral support by the contralateral hind (until touch-down of the reference hind at the 100% mark). Further description of movements is in reference to an average stride cycle of the left hindlimb and corresponds to Fig. 3.

Table 3. Mean ± s.d. intervertebral angles and pelvic displacements of reference hindlimb (rounded to full degrees) at touch-down and lift-off in *Choloepus didactylus*

	Lateral bending	Sagittal bending	Long-axis rotation			
	Touch-down angle (deg)	Lift off angle (deg)	Touch-down angle (deg)	Lift-off angle (deg)	Touch-down angle (deg)	Lift-off angle (deg)
6th presacral joint	–1±1	0±1	1±1	1±0	0±1	0±0
5th presacral joint	–2±1	1±1	1±1	1±1	–2±1	0±1
4th presacral joint	–2±1	1±2	4±2	3±1	–4±3	2±2
3rd presacral joint	–3±1	3±0	5±2	4±1	–3±3	1±1
2nd presacral joint	–3±1	1±1	10 ±1	9±2	–1±2	1±1
Lumbo-sacral joint	–1±1	0±1	19±3	15±2	–1±1	1±1
Pelvic displacement	–14±4	9±4	41±9	33±6	–13±4	6±3

Intervertebral angular movements of the thoraco-lumbar spine during locomotion

Lateral bending

Lateral bending movement patterns obtained for the six presacral intervertebral joints were monophasic over the course of a stride cycle (Figs 3, 4). At touch-down of the left hindlimb, additive intervertebral movement bent the thoraco-lumbar spine towards the left side of the body (negative values for lateral bending; Table 3). At touch-down of the right hindlimb, the thoraco-lumbar spine is bent maximally towards the right side of the body (positive values for lateral bending; Fig. 3). Amplitudes of lateral bending increased from the lumbo-sacral joint to the third presacral joint, at which the greatest amplitude was observed, and then decreased gradually in the more cranial intervertebral joints (Fig. 5). At the sixth presacral joint, only minimal lateral bending movements (<1 deg to either side) occur, which cannot be reliably detected with the non-invasive approach used in this study. On average, none of the six presacral joints analyzed had maximal amplitudes greater than 7 deg. No cranio-caudal pattern was observed in the timing of extreme angular displacements of individual intervertebral joints, as extreme lateral bending was observed approximately at limb touch-down (Table 4) and the instant of the stride cycle in which the extreme was reached varied between trials. Moreover, phases of bilateral hindlimb support were marked by comparatively little lateral bending movement (Fig. 3).

Sagittal bending

The sagittal bending movements measured in the six presacral intervertebral joints were biphasic over the course of a step cycle (Figs 3, 4). At hindlimb touch-down, the thoraco-lumbar spine is maximally flexed (higher values for sagittal bending; Table 3). Minima are associated with instants of hindlimb lift-off but, on average, these minima occur slightly after the lift-off event (Table 4). Sagittal bending amplitudes were highest at the lumbo-sacral joint and decreased gradually in a cranial direction, although we observed slightly higher sagittal bending movements at the fourth presacral joint than at the third presacral joint (Fig. 5). Again, no clear cranio-caudal pattern was observed in the timing of extreme angular displacements of individual intervertebral joints during an average stride cycle (Table 4).

Long-axis rotation

The long-axis rotation movement patterns of vertebrae at the six analyzed presacral joints were monophasic (Figs 3, 4). Clockwise rotation (as seen from cranial) along the long axis of the vertebral column is maximal approximately at the instant of touch-down of the left hindlimb (negative values for long-axis rotation; Table 3). After touch-down of the left hindlimb, counterclockwise long-axis rotation set in, which reached its maximum approximately at the instant of right hindlimb touch-down, after which clockwise rotation set in again. Amplitudes of intervertebral long-axis rotation increase until the fourth presacral joint, where the maximal mean amplitude of 7 deg was observed (Fig. 5). Intervertebral angular amplitudes during a stride cycle were much smaller at the fifth presacral joint and too small to be reliably detected at the sixth presacral joint. As in the case of the lateral bending and sagittal bending movement patterns, we did not observe a temporal cranio-caudal pattern of intervertebral long-axis rotation (Table 4).

Resulting pelvic displacements

The small intervertebral angular movements we observed are associated with pelvic displacements (Figs 3, 4). Mean amplitudes of 28, 9 and 27 deg occur for lateral displacement and sagittal protraction/retraction and long-axis rotation, respectively. Most of the observed pelvic displacement can be directly attributed to the summation of intervertebral movements measured at the thoraco-

Table 4. Percentage of stride cycle at which maximum and minimum angular displacements (rounded to full percent) follow touch-down of reference hindlimb in *Choloepus didactylus*

	Lateral bending		Sagittal bending*		Long-axis rotation	
	Max. (%)	Min. (%)	Max. (%)	Min. (%)	Max. (%)	Min. (%)
6th presacral joint	68±4	95±3	51±3	23±4	54±5	3±4
5th presacral joint	45±4	3±6	51±5	23±3	51±4	98±6
4th presacral joint	54±6	3±4	51±5	28±4	62±6	3±4
3rd presacral joint	54±5	8±5	60±5	31±2	45±4	3±5
2nd presacral joint	56±6	85±5	53±4	28±3	54±3	99±5
Lumbo-sacral joint	56±4	95±5	45±3	23±2	56±5	3±6
Pelvis	56±8	100±6	48±5	25±2	54±6	100±6

In some cases maxima are reached after touch-down (early in respect to reference contact phase).
*For the biphasic sagittal bending, only the first maximum and minimum of an average stride cycle are reported.
Data are means ± s.d.

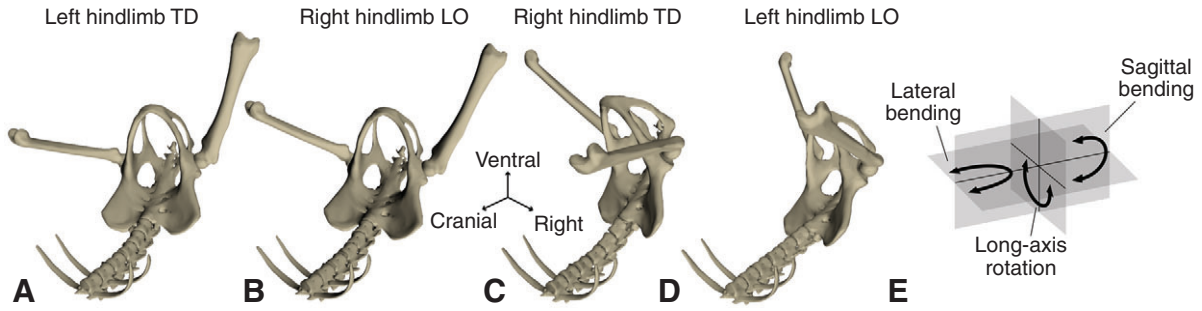

Fig. 4. Representative XROMM images of the thoraco-lumbar spine, the pelvis and the right femur, illustrating the principal movements occurring during trot-like quadrupedal locomotion of sloths at different instants of the stride cycle (A–D). Lateral displacement of the pelvis is maximal to either side of the body at touch-down (TD) of the hindlimb of the same side of the body and lateral displacement is maintained until contralateral lift-off (LO). Sagittal bending and rotation about the long-axis of the spine are less pronounced. Maximal sagittal flexion occurs at TD of each hindlimb, whereas maximal sagittal extension occurs at LO of each hindlimb. Both flexion and extension occur twice in a complete stride cycle and sagittal bending is thus biphasic. Long-axis rotation is maximal at TD of a hindlimb and rotates the hip of the same side of the body closer to the support. (E) Principal movements of the vertebral column (adapted from Schilling et al., 2005).

lumbar spine. The summation of the lateral bending movements of the six presacral joints analyzed accounted for 85.2% of the observed mean amplitude of lateral pelvic displacement. Likewise, sagittal bending movements in the thoraco-lumbar spine accounted for 90.8% of the observed maximal amplitude of the sagittal displacement of the pelvis. Together, the long-axis rotation movements of the six caudal-most presacral joints accounted for 77.2% of the long-axis rotation observed at the pelvis.

Over the course of a complete stride cycle, the pelvis is displaced in such a way that at left hindlimb touch-down it is maximally displaced towards the left side, maximally protracted in its sagittal plane and rotated so that the left hip joint is placed closer to the support. Little lateral displacement results in the hip joint being positioned directly under the foothold when the pelvis is progressed under the foot during the left contact phase. At right hindlimb lift-off, the pelvis is maximally retracted in its sagittal plane, but lateral displacement remains close to the value of left hindlimb touch-down. During right swing, the pelvis is displaced laterally and rotated about its long axis towards the right side of the body, again protracted in its sagittal plane (Fig. 4). Apart from the protraction, the pelvis maintains this approximate orientation until left hindlimb lift-off. During the left hindlimb's swing phase, the pelvis swings and rotates back to the left side of the body.

Femoral movements relative to the pelvis

Femoral movements consist of protraction and retraction, abduction and adduction, and rotation about the long axis. These movements are determined relative to the pelvis using an anatomical coordinate system placed at the hip joint. At touch-down, the femur is retracted approximately 60 deg (Fig. 6A) from the position parallel to the pelvic long axis used as the zero point for femoral rotations (Table 2). During the initial third of the contact phase, no significant retraction was observed, but during the last two-thirds of contact the femur is continuously retracted to approximately 120 deg until lift-off. During the swing phase, the femur is protracted again. The mean amplitude of femoral protraction and retraction was 57 deg over the stride cycle.

By contrast, the degree of abduction was clearly influenced by pelvic orientation at touch down of the hindlimbs (Fig. 6B). Relative to the pelvis, the femur was abducted by 31 deg on average (–31 deg rotation about the *y*-axis of the anatomical coordinate system placed at the femoral pivot). During the contact phase, abduction decreases and reaches a minimum at the instant of contralateral touch-down (*ca*. –25 deg). Abduction then increases again until completion of the ipsilateral contact phase and throughout the ipsilateral swing phase. It reaches a maximum at touch-down of the ipsilateral

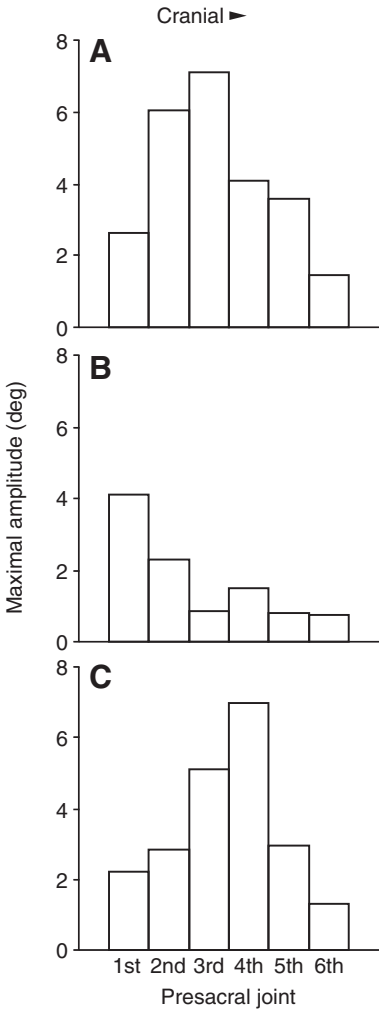

Fig. 5. Maximal mean amplitudes of intervertebral movements for individual intervertebral joints over the course of a stride cycle of a reference hindlimb in *Choloepus didactylus* (*N*=20). (A) Lateral bending; (B) sagittal bending; (C) long-axis rotation.

hindlimb. The overall mean amplitude of abduction/adduction was 7 deg.

The cranial surface of the femur is rotated outward about its long axis throughout the stride cycle (Fig. 6C). This outward rotation increases between touch-down and lift-off by approximately 8 deg on average. After reaching its maximum at lift-off, the outward rotation of the femoral long axis decreases again and reaches its minimum shortly prior to touch-down. We determined the mean overall amplitude of long-axis rotation to be 7 deg.

Influence of pelvic displacements on the trajectory of the knee

During normal locomotion, knee displacement has a mean medio-lateral amplitude of 3.9 cm (Fig. 7). If all of the pelvic rotations are turned off, medio-lateral displacement increases to 5.7 cm. Pelvic roll has a particularly drastic influence on medio-lateral displacement, which increases to over 8 cm if pelvic roll is muted in the virtual experiment. In sum, pelvic rotations over the course of the stride cycle facilitate a relatively linear retraction of the knee, without extensive medio-lateral excursions.

During normal locomotion, the knee has a cranio-caudal displacement amplitude of approximately 23.5 cm. If all pelvic rotations are turned off, this value decreases to less than 14 cm. Pelvic tilt, lateral displacement and sagittal protraction/retraction all contribute similarly to the cranio-caudal displacement of the knee, with the biggest influence exerted by pelvic protraction/retraction (Fig. 7).

The amplitude of dorso-ventral displacement of the knee over the course of a stride cycle is approximately 5.1 cm. If pelvic rotations are muted, this value decreases slightly. It is interesting to note that the muting of pelvic tilt actually increases the dorso-ventral displacement of the knee, but this effect is contradicted by the effect of pelvic lateral displacement and pelvic protraction/retraction.

DISCUSSION

Morphology of the thoraco-lumbar spine in relation to observed motion

The order Xenarthra is characterized by xenarthrous articulations in the thoraco-lumbar spine which, it has been argued, restrict the long-axis rotation of the vertebral column (Kraft, 1995; Endo et al., 2009), although Gaudin and Biewener found no significant differences from opossums when they subjected the thoraco-lumbar spine of an armadillo to torsion and ventral bending (Gaudin and Biewener, 1992). However, two-toed sloths do not have distinct xenarthrous articulations (Kraft, 1995). The parasagittally orientated articulating facets at the anterior zygapophyses of the lumbar vertebrae and last thoracic vertebra present in the sloth are also found in other species, including humans, and have also been argued to restrict extensive long-axis rotation and lateral bending (see Rockwell et al., 1938; Boszczyk et al., 2001; Benninger et al., 2006). As shown here for the sloth, small additive intervertebral motions can result in considerable long-axis rotation and lateral displacement of the pelvis even when the zygapophyses are thus configured. Pridmore also found that lateral bending in the postdiaphragmatic spine (i.e. between those vertebrae with parasagittal orientation of the zygapophyses) was similar to that of the prediaphragmatic spine (vertebrae with horizontal zygapophysal orientation) in a cineradiographic study on lateral bending in *Monodelphis* (Marsupialia) (Pridmore, 1992). As a result, the available cineradiographic data on symmetrical gaits in mammals do not clearly reflect the differences in mobility that might be expected on the basis of the articular features.

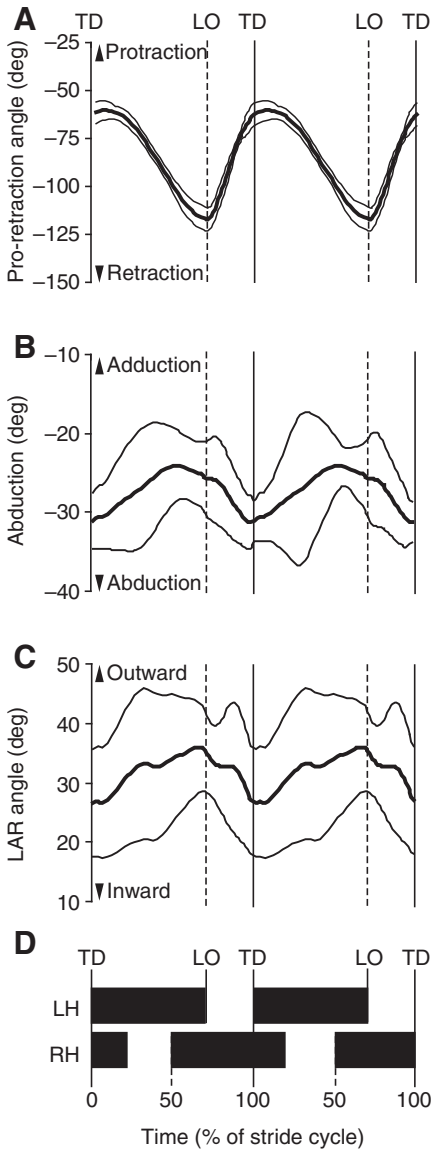

Fig. 6. Mean ± s.d. angular rotations at the femoral fulcrum (N=20) relative to two consecutive average stride cycles in *Choloepus didactylus*. (A) Femoral protraction and retraction; (B) femoral abduction; (C) femoral long-axis rotation (LAR); (D) Timing of contact phases (black boxes) and swing phases (white space between boxes) during two mean stride cycles of the left hindlimb (LH) and right hindlimb (RH). LO, lift-off; TD, touch-down.

According to Slijper, long spinal processes result in advantageous lever arms for muscles that sagittally extend the vertebral column (Slijper, 1946). This feature is thus often found in species that are able to gallop at high velocities and that display powerful sagittal extension (Slijper, 1946). The two-toed sloth has very short spinal processes and correspondingly only a thin layer of muscle. Moreover, Slijper claims that cranially directed spinal processes are better suited to extending the spine in the sagittal plane, whereas caudally directed spinal processes are favorable for long-axis rotation *via* the mm. rotatores and for effective lateral bending (Slijper, 1946). Accordingly, Curtis observed caudally directed

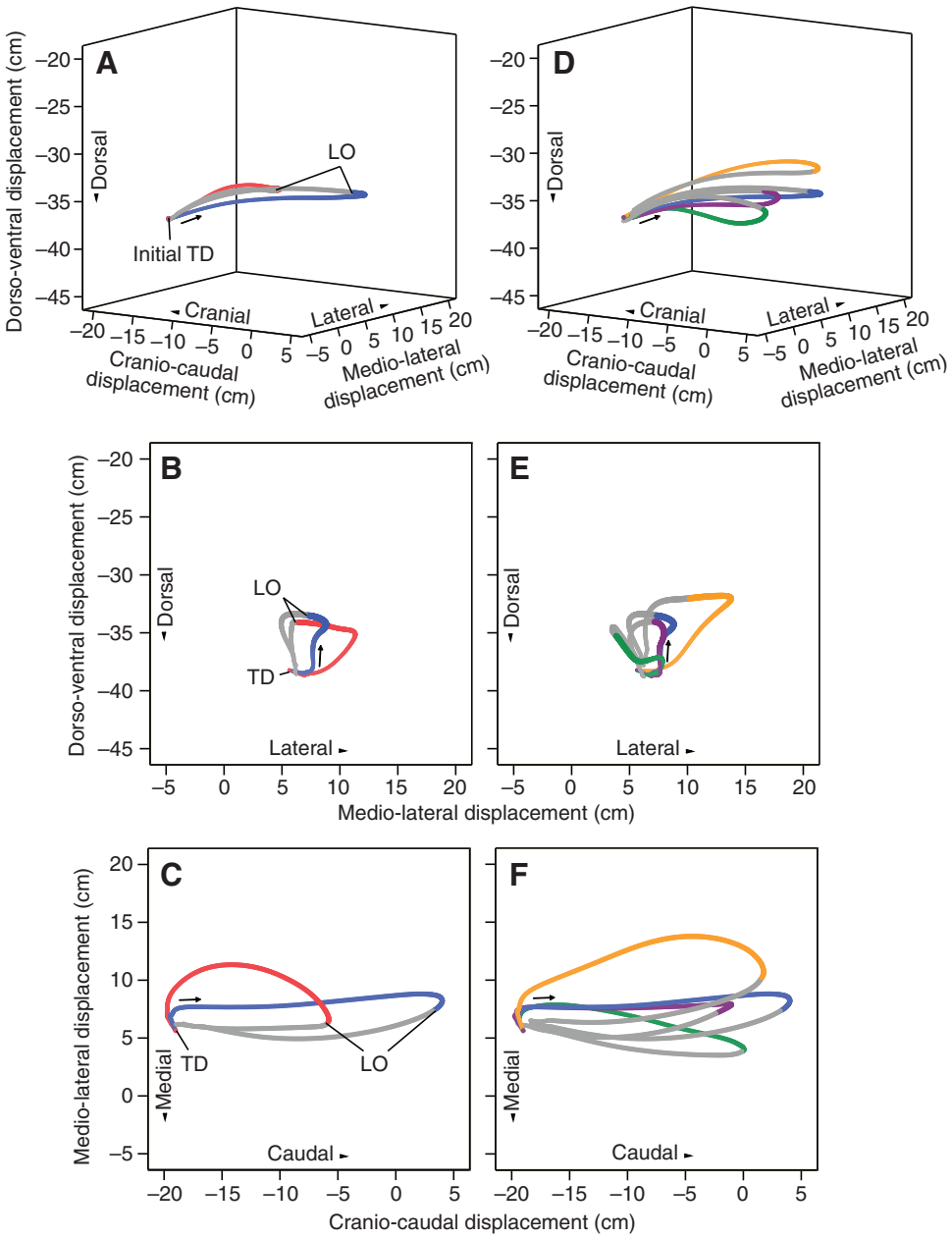

Fig. 7. Trajectories of the right knee and the influence of pelvic rotations in *Choloepus didactylus*. (A,D) 3-D trajectories; (B,E) trajectories from a caudal perspective; (C,F) trajectories from a ventral perspective. Arrows indicate the direction of knee displacement. Blue, normal locomotion; red, all pelvic rotations turned off; yellow, pelvic roll turned off; green, pelvic yaw turned off; purple, pelvic pitch turned off; grey, swing phases. LO, lift-off; TD, touch-down.

spinal processes in the slow loris (*Nycticebus coucang*) (Curtis, 1995), a species that is unable to gallop and that is characterized by extensive lateral bending during locomotion (Demes et al., 1990; Shapiro et al., 2001). Because sloths do not display asymmetrical gaits (Mendel, 1981; Nyakatura et al., 2010), the combination of a reduction in the overall muscle mass of the epaxial musculature and a reduction in the height of the caudally directed spinal processes thus conforms to expectations formed on the basis of previous findings.

3-D thoraco-lumbar spine movements and pelvic displacements

3-D thoraco-lumbar spine movements mostly conformed to the expectations we had formed on the basis of published data on the symmetric gaits of other mammalian quadrupeds. The lateral bending of the thoraco-lumbar spine and associated pelvic lateral displacements were monophasic. The maximal pelvic displacement to either side was reached at approximately hindlimb touch-down. This pattern has also been observed in *Monodelphis* (Pridmore, 1992), tree-shrews (Schilling and Fischer, 1999), various primate species (Shapiro et al., 2001; Schmidt, 2005), three carnivoran species (Jenkins and Camazine, 1977) and horses (Faber et al., 2000). Between touch-down of the reference hindlimb and that of the contralateral hindlimb, the amplitude of pelvic lateral bending was 28 deg. It is tempting to hypothesize that pronounced lateral displacements of the pelvis are related to arboreal locomotion, where hindlimbs need to be placed on supports that are smaller in diameter than the pelvis. But the data available on pelvic displacements owing to lateral bending of the spine in other species do not support this notion. Although similar lateral pelvic displacement was found in six strepsirrhine primate species (between 14 deg in *Loris tardigradus* and 37 deg in *Nycticebus coucang*) (Shapiro et al., 2001), values for more terrestrial species vary between 8 deg in tree-shrews (Schilling and Fischer, 1999) and 30–40 deg in *Monodelphis* (Pridmore, 1992). In an X-ray study on carnivoran pelvic displacements, Jenkins and Camazine observed just 13.5, 10.4 and

7.8 deg in raccoons, foxes and cats, respectively (Jenkins and Camazine, 1977), and van de Graaff et al. observed a lateral bending amplitude of 20 deg in the terrestrial skunk (*Mephitis mephitis*) (van de Graaff et al., 1982). Cursorial adaptations that markedly restrict parasagittal limb excursions are generally accompanied by relatively low lateral bending in the spine (cf. Jenkins and Camazine, 1977), but this does not explain the very low value found in the tree-shrew.

Intervertebral sagittal bending and the resulting displacement of the pelvis was biphasic and maxima of flexion were associated with touch-down events of the hindlimbs, whereas minima occurred at instances of hindlimb lift-off. This pattern was also observed in horses (Faber et al., 2000; Haussler et al., 2001), dogs (Ritter et al., 2001) and nine species of small quadrupedal mammals (Rocha Barbosa et al., 1996; Fischer et al., 2002) and seems to be a general characteristic of mammalian symmetric gaits. The maximal overall amplitude of pelvic displacement resulting from 3-D thoraco-lumbar spine motion was just 9 deg in this study, which is comparable to values for the eight small mammalian species studied by Fischer et al. (Fischer et al., 2002), which ranged from 7 deg in rats to 17 deg in kowaris, and to those for the guinea pig (16 deg) studied by Rocha-Barbosa et al. (Rocha-Barbosa et al., 1996).

The rotation about the long-axis of the pelvis resulting from 3-D thoraco-lumbar spine motion was monophasic as expected. Rotations to either side were maximal (and reduced the distance from the hip joint to the support) at hindlimb touch-down. Similar movement was described by Jenkins and Camazine (Jenkins and Camazine, 1977). A later study found maximal amplitudes of pelvic long-axis rotation in the tree-shrew of approximately 5 deg (Schilling and Fischer, 1999). Wennerstrand et al. observed mean long-axis rotation of 6 deg in the pelvis of sport horses (Wennerstrand et al., 2004). In the present study, a much larger amplitude of 27 deg was measured for the long-axis rotation of the sloth pelvis. Schmidt states that extensive lateral bending and twisting occurs in the lumbar spine of four small arboreal primate species during symmetric quadrupedal locomotion, but no quantitative data were provided (Schmidt, 2005). More comparative data are clearly needed to identify the conditions that influence the 3-D movements of the thoraco-lumbar region of the mammalian spine and the resulting pelvic displacements during symmetrical gaits.

Amplitudes of intervertebral angular deflections

In vitro studies show regional differences in intervertebral mobility (Yamamoto et al., 1989; Gaudin and Biewener, 1992; Fischer, 1994; Benninger et al., 2004). Studies on *in vivo* pelvic displacements alone cannot account for differences in mean angular deflection between individual intervertebral joints. Because only a fraction of maximal mobility is used during cyclic symmetric locomotion (e.g. Fischer, 1998), we cannot directly compare our *in vivo* data with *in vitro* data. Most published *in vivo* quantifications of regional differences in movements of the thoraco-lumbar spine averaged angular displacement over several vertebrae (Kafkafi and Golani, 1998; Faber et al., 2000; Shapiro et al., 2001; Wennerstrand et al., 2004; Gradner et al., 2007).

We expected the greatest individual amplitudes of presacral lateral bending, sagittal bending and long-axis rotation to be in the lumbo-sacral joint. This expectation was based on the results of the sole study to have analyzed more than one individual presacral joint *in vivo* during symmetric locomotion in a mammal (horse). Haussler et al. used an invasive method [similar to that employed by Wood et al. (Wood et al., 1992) and Schendel et al. (Schendel et al., 1995)], which involved a transducer being fixed firmly onto pins that were implanted in the vertebral bodies and protruded out of the skin, to directly measure the movement between the instrumented vertebrae during locomotion (Haussler et al., 2001). In our analysis of sloth locomotion, the position of maximal magnitude of intervertebral angular movement differs along the spine for the three rotations. This corresponds to *in vitro* data relating to humans (Yamamoto et al., 1989) and dogs (Benninger et al., 2004).

In contrast to the *in vivo* data collected by Haussler et al. for the horse (Haussler et al., 2001), we documented the highest magnitude of intervertebral lateral bending motion (~7 deg) to be at the third caudal-most presacral joint. Benninger et al. determined that the greatest amplitude occurred at the fourth caudal-most presacral joint (Benninger et al., 2004). Faber et al. found that the region of most pronounced angular lateral bending movement in horses at a slow walk occurred between vertebrae TH13 and TH17 (~4.3 deg; i.e. an mean of ~1.1 deg per joint) (Faber et al., 2000). The amplitudes of lateral bending in the individual intervertebral joints of the six strepsirrhine primate species analyzed by Shapiro et al. (Shapiro et al., 2001), which accounted for a lateral pelvic displacement of up to 37 deg, can be expected to be similar to those of the sloth.

In trot-like sloth locomotion, amplitudes of sagittal bending in individual presacral joints increased caudally, with the greatest magnitude occurring at the lumbo-sacral joint. This result corresponds to data from horses (Haussler et al., 2001; Wennerstrand et al., 2004), dogs (Benninger et al., 2004) and humans (Yamamoto et al., 1989).

Unlike in horses (Haussler et al., 2001), the maximal magnitude of long-axis rotation in sloths occurred at the fourth caudal-most presacral joint. The *in vitro* study on the lumbar spine in dogs revealed that long-axis rotation was greatest at the lumbo-sacral joint, but similar values were found at the fourth caudal-most prescaral joint as well (Benninger et al., 2004). Yamamoto et al. found the greatest range of motion *in vitro* in the third and fourth caudal-most presacral joints of humans (Yamamoto et al., 1989).

In sum, all of the studies that have investigated 3-D intervertebral movements in the lumbar spine have found that the greatest range of sagittal bending motion occurs at the lumbo-sacral joint, whereas the vertebral level of maximal lateral bending and long-axis rotation has differed among the species analyzed so far. Again, more comparative *in vivo* data are needed to test the generality of this observation.

Timing of maximal intervertebral angular deflections

Available data suggest that the presence of a cranio-caudal pattern in the maximal angular deflections of the spine depends on the gait sequence pattern. Kafkafi and Golani (Kafkafi and Golani, 1998) and Faber et al. (Faber et al., 2000) found that a traveling wave best describes the spinal lateral movements produced during the (lateral sequence) walking of ferrets and horses. According to Faber et al., the observed temporal cranio-caudal pattern of maximal intervertebral angular deflection offsets the phase differences between the hindlimbs and forelimbs, which are regarded as acting as a pivot point (Faber et al., 2000). Thus, no temporal cranio-caudal pattern of maximal intervertebral angular deflection should be present in trot-like gaits because diagonal forelimbs and hindlimbs are moved approximately synchronously and no phase differences occur (trots are further characterized by a standing wave of lateral spinal bending). Accordingly, a standing wave of lateral vertebral bending with nodes at the pectoral and pelvic girdle was observed in the walking trots of salamanders (Frolich and Biewener, 1992; Ashley-Ross, 1994) and lizards (Reilly and Delancey, 1997). In line with this, no cranio-caudal pattern of maximal angular deflections was observed in the thoraco-lumbar spine of sloths during trot-like

locomotion in this study, nor was it observed in trotting horses (Haussler et al., 2001).

Moreover, this hypothesis on the relationship between gait sequence pattern and an occurrence of a cranio-caudal pattern of maximal angular deflections is in line with published data on epaxial muscle activation. The cranio-caudal activation pattern of the epaxial muscles is consistent with a standing wave in trotting dogs and might represent a plesiomorphic pattern, owing to the comparable diagonal touch-down and lift-off events of the limbs also present in salamanders and lizards (Schilling and Carrier, 2010).

3-D femoral movements relative to the pelvis

Although the maxima and minima of protraction, retraction and long-axis rotation of the femur occurred approximately when touch-down and lift-off of the hindlimb was observed, abduction and adduction were clearly influenced by the pelvic position. Abduction was lowest at the moment of contralateral hindlimb touch-down, when the pelvis is maximally displaced and rotated (about its long axis) to the contralateral side, before abduction increases again prior to lift-off. At contralateral hindlimb touch-down, the ipsilateral hip joint (hindlimb pivot) is routed directly underneath the foot as the body is progressed under the support. Jenkins and Camazine observed a different pattern in their study of three carnivoran species, but recognized that femoral abduction during the contact phase and lateral displacement of the pelvis are interrelated components (Jenkins and Camazine, 1977). In these terrestrial species, femoral abduction was at a minimum at touch-down and increased until lift-off. Unfortunately, the authors did not provide precise data on the femoral movements observed during the short bipedal hindlimb support phase of the walking gaits studied. It can be assumed that, when forced to place their limbs on supports smaller than the diameter of their torso during arboreal locomotion, quadrupedal mammals exhibit more pronounced abduction/adduction movements over the course of a stride cycle than terrestrial ones. However, here too, more comparative data are required to test this hypothesis.

Kinematic studies of pelvic displacement during symmetric mammalian gaits have shown that the pelvis is displaced three-dimensionally (Jenkins and Camazine, 1977). Combined analysis of pelvic and femoral movements in the sloth shows that the knee trajectory results from displacements of the pelvis and movements of the femur relative to it, including long-axis rotation and adduction/abduction. To assess femoral motion relative to the pelvis, anatomical coordinate systems are necessary (e.g. Rubenson et al., 2007). Importantly, the observable trajectory of the knee and distal limb is almost linear during the contact phase of the sloth (cf. Fig. 7C). The 3-D kinematic data presented here thus hint at more complex muscular activity underlying femoral movement than might be deduced from the rather linear trajectory of the knee alone. If this also applies to other mammalian species, 3-D kinematic analyses should be helpful in interpreting EMG data or substrate reaction forces to infer limb function.

Conclusions

In short, caudally directed spinal processes and a thin epaxial muscle layer suggest that the thoraco-lumbar spine in sloths is not favorable for powerful extension in the sagittal plane, but probably facilitates lateral bending and long-axis rotation movements. The kinematic data do not reflect the differences in intervertebral mobility that would be expected on the basis of the configuration of the zygapophyses alone.

The 3-D *in vivo* kinematics of angular motion in the six caudal-most presacral joints, the resulting pelvic displacements and femoral movements relative to the pelvis did confirm some expectations that were based on the scant 3-D data available from previous publications. Owing to the consistency of the patterns of thoraco-lumbar lateral bending (monophasic), sagittal bending (biphasic) and long-axis rotation (monophasic) across diverse mammalian quadrupeds, they can be assumed to be part of a general pattern in mammalian symmetric gaits. Unlike in horses (going by the only comparable *in vivo* data), the maximal angular deflections associated with lateral bending and long-axis rotation did not occur at the lumbo-sacral joint. As in the other species investigated, no cranio-caudal pattern of maximal angular deflection was observed in the trot-like symmetrical gaits of sloths. We therefore hypothesize that a temporal cranio-caudal pattern of maximal intervertebral angular deflections is only present when forelimbs and hindlimbs move out of phase and spinal movement is best described as a traveling wave. It remains to be determined *via* EMG data on the epaxial muscles of the sloth whether pelvic displacements are the consequence of active bending of the spine or are the result of passive motion induced by the action of extrinsic hindlimb muscles, as proposed in relation to the more dynamic trotting of dogs (Schilling and Carrier, 2009). More generally, this relationship between active bending and passive displacement might depend on the speed of mammalian symmetrical locomotion. Femoral protraction and retraction and long-axis rotation are governed by the stride cycle of the leg, whereas abduction is related to the lateral displacement of the pelvis. Both pelvic displacement and femoral movements are complex. Quantifying them might allow us to make more differentiated inferences about hindlimb muscle function from EMG or substrate reaction force data. In arboreal species, more pronounced movements of the thoraco-lumbar spine are likely to facilitate the efficient retraction of the hindlimb during the contact phase when the foot is placed closer to the sagittal plane on narrow supports. More comparative data are required to shed more light on the spatial and temporal patterns in the intervertebral movements of the mammalian spine during symmetric gaits.

ACKNOWLEDGEMENTS

Without the XROMM short course in August 2009 held by the developers of the method at Brown University, Providence, RI, USA, this study would not have been possible. A. Petrovitch provided access to the medical CT scanner. I. Shappert generously provided the sloths Julius and Evita as a loan from Dortmund Zoo, Germany. E. Woker helped with animal keeping. R. Kraft of the Bayrische Staatssammlung, Munich, Germany, granted access to the museum collection. R. Petersohn and L. Wagner helped with the experiments. H. Stark developed the software that was used to convert the file formats of the different 3-D software packages. N. Schilling formulated helpful criticism on an earlier version of the manuscript. L. Cathrow thoroughly edited the language. The study was financially supported by the Deutsche Forschungsgemeinschaft (grant DFG Fi 410/11-1 to M.S.F.).

REFERENCES

Ashley-Ross, M. (1994). Hindlimb kinematics during terrestrial locomotion in a salamander (*Dicamptodon tenebrosius*). *J. Exp. Biol.* **193**, 255-283.

Benninger, M. I., Seiler, G. S., Robinson, L. E., Ferguson, S. J., Bonél, H. M., Busato, A. R. and Lang, J. (2004). Three-dimensional motion pattern of the caudal lumbar and lumbosacral portions of the vertebral column of dogs. *Am. J. Vet. Res.* **65**, 544-552.

Benninger, M. I., Seiler, G. S., Robinson, L. E., Ferguson, S. J., Bonél, H. M., Busato, A. R. and Lang, J. (2006). Effects of anatomic conformation on three-dimensional motion of the caudal lumbar and lumbosacral portions of the vertebral column of dogs. *Am. J. Vet. Res.* **67**, 43-50.

Boszczyk, B. M., Boszczyk, A. A. and Putz, R. (2001). Comparative and functional anatomy of the mammalian lumbar spine. *Anat. Rec.* **264**, 157-168.

Brainerd, E. L., Baier, D. B., Gatesy, S. M., Hedrick, T. L., Metzger, K. A., Gilbert, S. L. and Crisco, J. J. (2010). X-ray reconstruction of moving morphology (XROMM): precision, accuracy and application in comparative biomechanics research. *J. Exp. Zool.* **313A**, 262-279.

Curtis, D. (1995). Functional anatomy of the trunk musculature in the slow loris (*Nycticebus coucang*). *Am. J. Phys. Anthropol.* **97**, 367-379.

Demes, B., Jungers, W. L. and Nieschalk, U. (1990). Size- and speed-related aspects of quadrupedal walking in slender and slow lorises. In *Gravity, Posture and*

Locomotion in Primates (ed. F. K. Jouffroy, M. H. Stack and C. Niemitz), pp. 175-198. Firenze: Editrice II Sedicesmo.

Endo, H., Komiya, T., Kawada, S., Hayashida, A., Kimura, J., Itou, T., Koie, H. and Sakai, T. (2009). Three-dimensional reconstruction of the xenarthrous process of the thoracic and lumber vertebrae in the giant anteater. *Mammal Study* **34**, 1-6.

Faber, M., Schamhardt, H., van Weeren, R., Johnston, C., Roepstorff, L. and Barneveld, A. (2000). Basic three-dimensional kinematics of the vertebral column of horses walking on a treadmill. *Am. J. Vet. Res.* **61**, 399-406.

FCAT (2008). *Terminologica Anatomica*, pp. 1-292. Stuttgart: Thieme Verlag.

Fischer, M. S. (1994). Crouched posture and high fulcrum, a principle in the locomotion of small mammals: the example of the rock hyrax (*Procavia capensis*) (Mammalia: Hyracoidea). *J. Hum. Evol.* **26**, 501-524.

Fischer, M. S. (1998). Die Lokomotion von Procavia Capensis (Mammalia, Hyracoidea): Zur Evolution des Bewegungssystems bei Säugetieren. *Abhandlungen des Naturwissenschaftlichen Vereins in Hamburg* **33**, 1-188 (in German).

Fischer, M. S., Schilling, N., Schmidt, M., Haarhaus, D. and Witte, H. (2002). Basic limb kinematics of small therian mammals. *J. Exp. Biol.* **205**, 1315-1338.

Flower, W. H. (1882). On the mutual affinities of the animals composing the order Edentata. *Proc. Zool. Soc.* **50**, 358-367.

Frolich, L. M. and Biewener, A. A. (1992). Kinematic and electromyographic analysis of the functional role of the body axis during terrestrial and aquatic locomotion in the salamander *Ambystoma Tigrinum*. *J. Exp. Biol.* **162**, 107-130.

Gatesy, S. M., Baier, D. B., Jenkins, F. A. and Dial, K. P. (2010). Scientific rotoscoping: a morphology-based method of 3-D motion analysis and visualization. *J. Exp. Zool.* **313A**, 262-279.

Gaudin, T. J. and Biewener, A. A. (1992). The functional morphology of xenarthrous vertebrae in the armadillo *Dasypus novemcinctus* (Mammalia, Xenarthra). *J. Morphol.* **214**, 63-81.

Gaudin, T. J. and McDonald, H. G. (2008). Morphology-based investigations of the phylogenetic relationships among extant and fossil xenarthrans. In *The Biology of the Xenarthra* (ed. S. F. Vizcaíno and W. J. Loughry), pp. 24-36. Gainesville: University Press of Florida.

Gradner, G., Bockstahler, B., Peham, C., Henninger, W. and Podbregar, I. (2007). Kinematic study of back movement in clinically sound malinois dogs with consideration of the effect of radiographic changes in the lumbosacral junction. *Vet. Surg.* **36**, 472-481.

Haussler, K. K., Bertram, J. E. A., Gellman, K. and Hermanson, J. W. (2001). Segmental in vivo vertebral kinematics at the walk, trot and canter: a preliminary study. *Equine Vet. J.* **Suppl. 33**, 160-164.

Howell, A. B. (1944). *Speed in Animals*. Chicago: University of Chicago Press.

Jenkins, F. A. and Camazine, S. M. (1977). Hip structure and locomotion in ambulatory and cursorial carnivores. *J. Zool. Lond.* **181**, 351-370.

Kafkafi, N. and Golani, I. (1998). A traveling wave of lateral movement coordinates both turning and forward walking in the ferret. *Biol. Cybern.* **78**, 441-453.

Kraft, R. (1995). Xenarthra. In *Handbuch der Zoologie*, Vol. 8 (Mammalia) (ed. J. Niethammer, H. Schliemann and D. Starck), pp. 1-79. Berlin: Walter de Gruyter and company.

Kubo, T. and Ozaki, M. (2009). Does pace angulation correlate with limb posture. *Paleogeogr. Paleoclimatol. Paleoecol.* **275**, 54-58.

Licka, T. F., Peham, C. and Zohmann, E. (2001). Treadmill study of the range of back movement at the walk in horses without back pain. *Am. J. Vet. Res.* **62**, 1173-1179.

Mendel, F. C. (1981). Use of hands and feet of two-toed sloths (*Choloepus hoffmanni*) during climbing and terrestrial locomotion. *J. Mammal.* **62**, 413-421.

Nyakatura, J. A. and Fischer, M. S. (2010). Three-dimensional kinematic analysis of the pectoral girdle during upside down locomotion of two-toed sloths (*Choloepus didactylus*, Linné 1758). *Front. Zool.* **7**, 21.

Nyakatura, J. A., Petrovitch, A. and Fischer, M. S. (2010). Limb kinematics during locomotion in the two-toed sloth (*Choloepus didactylus*, Xenarthra) and its implications for the evolution of the sloth locomotor apparatus. *Zoology* **113**, 221-234.

Pridmore, P. A. (1992). Trunk movements during locomotion in the marsupial *Mondelphis domestica* (Didelphidae). *J. Morphol.* **211**, 137-146.

Reilly, S. M. and Delancey, M. J. (1997). Sprawling locomotion in the lizard *Sceloporus clarkia*: the effects of speed on gait, hindlimb kinematics, and axial bending during walking. *J. Zool. Lond.* **241**, 417-433.

Ritter, D. A., Nassar, P. N., Fife, M. and Carrier, D. R. (2001). Epaxial muscle function in trotting dogs. *J. Exp. Biol.* **204**, 3053-3064.

Rocha-Barbosa, O., Renous, S. and Gasc, J. P. (1996). Comparison of the fore and hind limb kinematics in the symmetrical and asymmetrical gait of a caviomorph rodent, the domestic guinea pig, *Cavia procellus* (Linné, 1758) (Rodentia, Caviidae). *Ann. Sci. Nat. Zool. Paris* **13e**, 149-165.

Rockwell, H., Evans, F. G. and Pheasant, H. C. (1938). The comparative morphology of the vertebrate spinal column. Its form as related to function. *J. Morphol.* **63**, 87-117.

Rubenson, J., Lloyd, D. G., Besier, T. F., Heliams, D. B. and Fournier, P. A. (2007). Running in ostriches (*Struthio camelus*): three-dimensional joint axes alignment and joint kinematics. *J. Exp. Biol.* **210**, 2548-2562.

Schendel, M. J., Dekutoski, M. B., Ogilvie, J. W., Olsewski, J. M. and Wallace, L. J. (1995). Kinematics of the canine intervertebral joints. An *in vivo* study before and after adjacent instrumentation. *Spine* **20**, 2555-2564.

Schilling, N. and Carrier, D. R. (2009). Function of the epaxial muscles during trotting. *J. Exp. Biol.* **212**, 1053-1063.

Schilling, N. and Carrier, D. R. (2010). Function of the epaxial muscles in walking, trotting and galloping dogs: implications for the evolution of epaxial muscle function in tetrapods. *J. Exp. Biol.* **213**, 1490-1502.

Schilling, N. and Fischer, M. S. (1999). Kinematic analysis of treadmill locomotion of tree shrews, *Tupaia glis* (Scandentia: Tupaiidae). *Z. Säugetierk.* **64**, 129-153.

Schilling, N., Arnold, D., Wagner, H. and Fischer, M. S. (2005). Evolutionary aspects and muscular properties of the trunk –- implications for human low back pain. *Pathophysiol* **12**, 233-242.

Schmidt, M. (2005). Hind limb proportions and kinematics: are small primates different from other small mammals? *J. Exp. Biol.* **208**, 3367-3383.

Shapiro, L. Z., Demes, B. and Cooper, J. (2001). Lateral bending of the lumbar spine during quadrupedalism in strepsirhines. *J. Hum. Evol.* **40**, 231-259.

Slijper, E. J. (1946). Comparative biologic-anatomical investigations on the vertebral column and spinal musculature of mammals. *Kan. Ned. Akad. Wet. Verh.* (Tweede Sec.) **42**, 1-128.

Van de Graaff, K. M., Harper, J. and Goslow, G. E. (1982). Analysis of posture and gait selection during locomotion in the striped skunk (*Mephitis mephitis*). *J. Mammal.* **63**, 582-590.

Wennerstrand, J., Johnston, C., Roethlisberger-Holm, K., Erichsen, C., Eksell, P. and Drevemo, S. (2004). Kinematic evaluation of the back in the sport horse with back pain. *Equine Vet. J.* **36**, 707-711.

Wood, K. B., Schendel, M. J., Pashman, R. S., Butterman, G. R., Lewis, J. L., Ogilvie, J. W. and Bradford, D. S. (1992). In vivo analysis of canine intervertebral and facet motion. *Spine* **17**, 1180-1186.

Yamamoto, I., Panjabi, M. M., Crisco, T. and Oxland, T. (1989). Three-dimensional movements of the whole lumbar spine and lumbosacral joint. *Spine* **14**, 1256-1260.